AIP | Physics of Fluids

Nonlinear oscillations following the Rayleigh collapse of a gas bubble in a linear viscoelastic (tissue-like) medium

Chengyun Hua and Eric Johnsen

Citation: Phys. Fluids **25**, 083101 (2013); doi: 10.1063/1.4817673
View online: http://dx.doi.org/10.1063/1.4817673
View Table of Contents: http://pof.aip.org/resource/1/PHFLE6/v25/i8
Published by the AIP Publishing LLC.

PHYSICS OF FLUIDS **25**, 083101 (2013)

Nonlinear oscillations following the Rayleigh collapse of a gas bubble in a linear viscoelastic (tissue-like) medium

Chengyun Hua[1,a)] and Eric Johnsen[2,b)]
[1]*Division of Engineering and Applied Science, California Institute of Technology, 1200 E. California Blvd., Pasadena, California 91125, USA*
[2]*Department of Mechanical Engineering, University of Michigan, 1231 Beal Ave., Ann Arbor, Michigan 48109, USA*

(Received 29 October 2012; accepted 22 July 2013; published online 13 August 2013)

In a variety of biomedical engineering applications, cavitation occurs in soft tissue, a viscoelastic medium. The present objective is to understand the basic physics of bubble dynamics in soft tissue. To gain insights into this problem, theoretical and numerical models are developed to study the Rayleigh collapse and subsequent oscillations of a gas bubble in a viscoelastic material. To account for liquid compressibility and thus accurately model large-amplitude oscillations, the Keller-Miksis equation for spherical bubble dynamics is used. The most basic linear viscoelastic model that includes stress relaxation, viscosity, and elasticity (Zener, or standard linear solid) is considered for soft tissue, thereby adding two ordinary differential equations for the stresses. The present study seeks to advance past studies on cavitation in tissue by determining the basic effects of relaxation and elasticity on the bubble dynamics for situations in which compressibility is important. Numerical solutions show a clear dependence of the oscillations on the viscoelastic properties and compressibility. The perturbation analysis (method of multiple scales) accurately predicts the bubble response given the relevant constraints and can thus be used to investigate the underlying physics. A third-order expansion of the radius is necessary to accurately represent the dynamics. Key quantities of interest such as the oscillation frequency and damping, minimum radius, and collapse time can be predicted theoretically. The damping does not always monotonically decrease with decreasing elasticity: there exists a finite non-zero elasticity for which the damping is minimum; this value falls within the range of reported tissue elasticities. Also, the oscillation period generally changes with time over the first few cycles due to the nonlinearity of the system, before reaching an equilibrium value. The analytical expressions for the key bubble dynamics quantities and insights gained from the analysis may prove valuable in the development and optimization of certain biomedical applications. © *2013 AIP Publishing LLC*. [http://dx.doi.org/10.1063/1.4817673]

I. INTRODUCTION

Cavitation plays an important role in a wide range of biomedical applications. To improve diagnostic ultrasound, attempts have been made to develop effective and safe contrast agents.[1] In therapeutic ultrasound, the destructive properties of cavitation are exploited to break kidney and gall stones (shock-wave lithotripsy[2]) or ablate pathogenic tissue (histotripsy[3]). In impact- and blast-induced traumatic brain injury, it has been suggested that cavitation inflicts mechanical damage.[4] Regardless of the specific area, cavitation in biomedical settings takes place in biological liquids or soft tissue, neither of which behaves as a Newtonian fluid. The challenge in studying cavitation in soft

a)Electronic mail: chua@caltech.edu
b)Electronic mail: ejohnsen@umich.edu

tissue lies in the viscoelastic, compressible, and multiphase nature of the problem. Direct simulations of the compressible equations of motion have been performed to study single-bubble dynamics in biomedical applications, many of which have been restricted to inviscid[5–8] and Newtonian[9] simulations. The few direct simulations in a viscoelastic medium are based on Maxwell fluids, none in which compressibility is included, preventing accurate studies of large-amplitude oscillations. Foteinopoulou and Laso[10] conducted finite element simulations of a bubble in a Phan-Thien-Tanner fluid and showed that oscillation amplitudes increased with increasing Deborah number. Lind and Phillips considered the collapse of a spherical bubble in a Maxwell fluid[11] and non-spherical collapse of a two-dimensional bubble in a weakly compressible upper-convected Maxwell fluid[12] using a boundary element method. Their results suggest that viscoelasticity has the ability to prevent jet formation and is likely to mitigate cavitation damage.

Useful insights into cavitation dynamics can be gained through the Rayleigh-Plesset equation,[13] a second-order nonlinear ordinary differential equation that describes the response of a single spherical bubble in an infinite and incompressible liquid subjected to a far-field pressure change. Subsequent extensions to the Rayleigh-Plesset equation have been developed to include compressibility, thermal and mass transfer effects, and non-spherical perturbations.[14] To distinguish between small-amplitude oscillations and violent collapse dominated by nonlinearity that is expected to be a substantial source of damage to the surroundings, Flynn[15,16] developed the idea of an inertial cavitation threshold. Past studies of bubble dynamics in viscoelastic media based on Rayleigh-Plesset approaches have primarily focused on polymeric liquids governed by Maxwell-like constitutive models.[17–20]

In the biomedical context, Allen and Roy[21,22] studied forced bubble oscillations in incompressible linear and nonlinear Maxwell fluids. They found significant differences between the viscoelastic and Newtonian cases and that subharmonic excitations at specific fluid parameters lead to a discrete group modulation of the radial excursion. Khismatullin and Nadim[23] investigated oscillations of a microbubble encapsulated in a viscoelastic shell in a slightly compressible viscoelastic liquid. They showed that the resonance frequency for the encapsulated microbubble depends on viscous damping and differs from the undamped natural frequency. Jimenez-Fernandez and Crespo[24] found that the influence of the rheological fluid properties on the pressure thresholds for inertial cavitation in an Oldroyd fluid were closely related. Yang and Church[25] implemented the Kelvin-Voigt model into the (compressible) Keller-Miksis equation to investigate forced bubble oscillations. They observed that elasticity increases the threshold pressure for inertial cavitation, and subharmonic signals may only be detectable in certain ranges of radius and pressure amplitude. This model was further used to investigate cavitation-induced bioeffects in contrast-enhanced ultrasound.[26] Brujan[27,28] considered compressible bubble dynamics in Maxwell and Jeffreys media and concluded that relaxation and retardation have little effects for Reynolds numbers beyond a certain value. Naude and Mendez[29] conducted Rayleigh-Plesset simulations with thermal diffusion in an upper-convected Maxwell liquid to show that chaotic behavior is observed beyond a certain Deborah number.

The present study seeks to advance these past studies on cavitation in tissue by determining the basic effects of relaxation and elasticity on the bubble dynamics for large-amplitude oscillations. For this purpose, a Zener viscoelastic model is considered in this work, which accounts for both creep and stress relaxation, in conjunction with liquid compressibility. A combined analytical and numerical approach is used to predict spherical bubble dynamics in a tissue-like medium following a Rayleigh collapse. The problem setup and governing equations are listed in Sec. II, followed by the theoretical analysis and numerical results in Sec. III. The article concludes with a summary and future directions.

II. PROBLEM SETUP AND EQUATIONS OF MOTION

A. Problem setup: Rayleigh collapse

The goal of the present study is to understand how elasticity and relaxation affect the dynamics of bubbles in a viscoelastic media in situations when compressibility is significant. Thus, a conceptually simple problem is considered, Rayleigh collapse,[30] i.e., the collapse of a bubble starting at its

maximum radius caused by the pressure difference between the surroundings and the interior. Here, a single bubble in an infinite homogeneous medium is considered. Historically, the problem is usually set up by instantaneously increasing the pressure of the surroundings by a value p_A.[13] The focus of the present work lies in this problem. Another means of perturbing the flow is to vary the initial radius about its equilibrium, which in turn modifies the bubble pressure (see Sec. III C). Contrary to problems in which the bubble is driven by an external harmonic pressure field, Rayleigh collapse has the advantage of having no time scale associated with the far-field pressure, thus reducing the parameter space.

B. Bubble dynamics: The Keller-Miksis equation

The dynamics of a single spherical gas bubble in an infinite body of compressible viscoelastic material are considered based on the Keller-Miksis equation[31–33]

$$\left(1-\frac{\dot{R}}{c_\infty}\right)R\ddot{R}+\frac{3}{2}\left(1-\frac{1}{3}\frac{\dot{R}}{c_\infty}\right)\dot{R}^2=\left(1+\frac{\dot{R}}{c_\infty}\right)\frac{p_B-p_\infty-p_A\left(t+\frac{R}{c_\infty}\right)}{\rho_\infty}+\frac{R}{\rho_\infty c_\infty}\dot{p}_B, \quad (1)$$

where $R(t)$ is the radius of the bubble, the dot denotes the time derivative, c_∞ and ρ_∞ are the sound speed and density of the surrounding medium, p_∞ is the constant far-field pressure, and $p_A(t+R/c_\infty)\approx p_A(t)+(R/c_\infty)\dot{p}_A$ is the time-varying far-field component. In the incompressible limit $c_\infty\to\infty$, Eq. (1) reduces to the well-known Rayleigh-Plesset equation for bubble dynamics in an incompressible medium. The Keller-Miksis equation provides a mechanism for acoustic radiation important in large-amplitude oscillations (e.g., inertial cavitation) relevant to the problems under consideration, but is still based on the idea that the near-field is incompressible.[31] The equation is valid to first order in the Mach number.

Since Rayleigh collapse is considered, p_A is a constant step increase in pressure. The pressure on the liquid side of the interface p_B is given by balancing the normal stresses across the interface

$$p_B=p_i-\frac{2\sigma}{R}+3\int_R^\infty\frac{\tau_{rr}(r)}{r}dr, \qquad p_i=p_{Go}\left(\frac{R_o}{R}\right)^{3\gamma}, \qquad p_{Go}=p_\infty+\frac{2\sigma}{R_o}, \quad (2)$$

where σ is the surface tension, τ_{rr} is rr-component of the viscous stress tensor (traceless, as discussed in Allen and Roy[22]), p_i is the internal pressure, R_o is the initial radius, p_{Go} is the initial partial pressure of non-condensible gas (air) in the bubble, and the polytropic index is $\gamma=1.4$ assuming adiabatic behavior. Although vapor pressure could be included as a constant in Eq. (2), it is neglected here. Surface tension and non-condensible gas are included, but their dependence is not explored.

C. Tissue constitutive model and properties: The Zener viscoelastic model

To close the system (1) and (2), a constitutive relation between the stresses τ_{rr} and strains

$$\gamma_{rr}(r)=\int_0^t\frac{\partial u}{\partial r}dt'=-\frac{2}{3}\frac{R^3-R_o^3}{r^3}, \quad (3)$$

is needed. Although its microstructure is typically heterogeneous,[34] tissue here is assumed to effectively behave as a homogeneous viscoelastic whole, with uniform and constant macroscopic properties. Tissue exhibits viscosity μ, shear modulus G (which will be referred to as elasticity henceforth) in the form of a restoring force, and relaxation λ, i.e., it takes a finite time to recover its initial configuration after applying a displacement.[34] Given that the goal is to understand the basic effects of these viscoelastic properties on the bubble dynamics, a linear Zener[35] (or standard linear solid) model is considered to represent tissue for simplicity, based on the following generalized relationship:

$$\lambda\frac{\partial\tau_{rr}}{\partial t}+\tau_{rr}=2G\gamma_{rr}+2\mu\frac{\partial\gamma_{rr}}{\partial t}. \quad (4)$$

The Zener model is the simplest model of a viscoelastic solid that predicts both creep and stress relaxation. Such models have been used to model various soft tissues,[36] although not in the context of

TABLE I. Different limits of the linear viscoelastic model Eq. (4).

Model	Properties	Equation
Kelvin-Voigt	$\lambda = 0$	$\tau_{rr} = 2G\gamma_{rr} + 2\mu\dot{\gamma}_{rr}$
Maxwell	$G = 0$	$\lambda\dot{\tau}_{rr} + \tau_{rr} = 2\mu\dot{\gamma}_{rr}$
Zener	...	$\lambda\dot{\tau}_{rr} + \tau_{rr} = 2G\gamma_{rr} + 2\mu\dot{\gamma}_{rr}$

cavitation. As shown in Table I, an appropriate definition of the coefficients reduces Eq. (4) to other known viscoelastic models: Kelvin-Voigt is recovered if $\lambda \to 0$. When $G = 0$, the Maxwell model is obtained; Oldroyd-like models have also been considered in the past for cavitation in polymeric solutions.[27]

In the Zener model (Fig. 1), μ, λ, and G are apparent properties that are not independent of each other, as evidenced by expressing these parameters in terms of a spring (G_2) in series with a dashpot (η), in parallel with another spring (G_1) In Eq. (4), these coefficients correspond to $\lambda = \eta/G_2$, $G = G_1$, and $\mu = \frac{\eta}{G_2}(G_1 + G_2)$. The quantities λ and μ/G_1 are characteristic times that correspond to relaxation for constant strain and constant stress, respectively.[34] To be physical, all spring and damping coefficients must be positive, which set a constraint on G_2

$$G_2 = \frac{\mu}{\lambda} - G_1 > 0, \qquad \text{or} \quad \frac{\mu}{\lambda} > G. \tag{5}$$

Equation (5) must be satisfied for a physically meaningful result, and it will be shown that this constraint naturally assists the analysis in Secs. II E and III B. Failing to meet this constraint, e.g., by independently selecting μ, G, and λ, may lead to unexpected behavior, some of which is described in the Appendix. For instance, a negative G_2 may be achieved with an incorrect set of parameters, thus leading to never-ending oscillations despite obvious damping mechanisms.

For relevance to biomedical applications, material properties representative of soft tissue are considered. Large variations in these properties are found in the literature. The acoustic properties of tissue (sound speed, density) are taken to be equal to those of water since they are similar for a wide range of tissues.[37,38] The surface tension for blood and air is taken from Apfel and Holland[39] and the viscosity from Yang and Church.[25] The elasticity of tissue is assumed to span $G = 0 - 10$ MPa,[40,41] with upper values corresponding to atherosclerotic tissue.[42] A wide range of relaxation times have been reported,[43,44] which usually depend on the loading; mathematically meaningful relaxation times, satisfying Eq. (5), are considered. The amplitude of the instantaneous pressure increase is fixed at $p_A = 3.4$ MPa to correspond to the pressure ratio driving the collapse of a vapor-filled bubble. The dimensionless parameters are constructed using the density of the surrounding medium ($\rho_\infty = 1060$ kg/m^3), characteristic initial radius ($R_o = 5$ μm), and velocity $c_o = \sqrt{p_\infty/\rho_\infty}$ chosen such that the non-dimensional ambient pressure is unity. Thus, the characteristic time is approximately the collapse time. The relevant dimensionless parameters are listed in Table II. The present focus is to understand how the Cauchy number (inertia vs. elasticity) and Deborah number (relaxation vs. inertia) affect the bubble dynamics; thus, the bubble response is computed as these numbers are varied. All the other non-dimensional parameters are held constant: C (compressibility), Weber number (surface tension vs. inertia) and Reynolds number (viscous forces vs. inertia), and the gas constant.

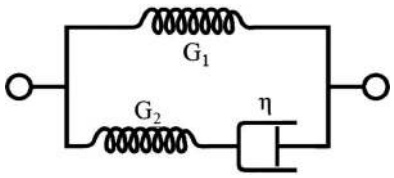

FIG. 1. Spring-dashpot schematic for the Zener model. Springs are denoted by spring constants G_i, and the dashpot by damping coefficient η.

TABLE II. Properties of the surrounding medium (representative of soft tissue) used in the present work. The bubble response is evaluated as Ca and De are varied, with $De/Ca < 1/Re$; all other non-dimensional parameters are held constant unless otherwise mentioned.

Property	Nominal value	Dimensionless expression/value	(Parameter)
Ambient pressure	$p_{\text{atm}} = 1$ atm	$1 = p_{\text{atm}}/\rho_\infty c_o^2 = 1.0$	
Pressure increase	$p_A = 3.4$ MPa	$p_R = p_A/\rho_\infty c_o^2 = 34$	
Sound speed	$c = 1540$ m/s	$C = c/c_o = 160$	
Surface tension	$\sigma = 0.056$ N/m	$We = R_o\rho_\infty c_o^2/\sigma = 9.0$	(Weber number)
Viscosity	$\mu = 0.015$ Pa s	$Re = R_o\rho_\infty c_o/\mu = 3.0$	(Reynolds number)
Elasticity	$G = 0 - 10$ MPa	$Ca = \rho_\infty c_o^2/G > 0.01$	(Cauchy number)
Relaxation time	$\lambda \leq 0.5\ \mu$s	$De = \lambda c_o/R_o \leq 1$	(Deborah number)

The present Zener model is arguably the simplest fluid and solid viscoelastic model, as it combines a Hookean solid with a Newtonian fluid. More sophisticated models of relevance to soft tissue mechanics include frequency-dependent coefficients, finite deformation, and nonlinear viscoelasticity.[34] Although adding compressibility to more accurately represented large-amplitude dynamics constitutes one of the advances of this work, it should be noted that large strains may require finite-strain analysis[45] and/or nonlinear viscoelasticity,[46] as opposed to the linear models used here. Furthermore, large-amplitude oscillations are prone to non-spherical perturbation growth.[47] While all potentially interesting, these research questions fall beyond the scope of the present study.

D. Coupling of the constitutive relation to the bubble dynamics

The constitutive relation is coupled to the Keller-Miksis equation through Eq. (2). To provide closure, Eq. (4) is integrated from R to infinity. For constant properties and using Leibniz' rule,

$$\lambda\dot{\varsigma} + \varsigma + \lambda\frac{\dot{R}}{R}\tau_{rr}|_R = \frac{1}{3}\left[-\frac{4}{3}G\left(1 - \frac{R_o^3}{R^3}\right) - 4\mu\frac{\dot{R}}{R}\right], \qquad \text{where } \varsigma = \int_R^\infty \frac{\tau_{rr}(r,t)}{r}dr. \tag{6}$$

Since the stress at the bubble wall $\tau_{rr}|_R$ is required in Eq. (6), an additional equation for this quantity must be provided by evaluating Eq. (4) at $r = R$

$$\lambda\dot{\tau}_{rr}|_R + \tau_{rr}|_R = -\frac{4}{3}G\left(1 - \frac{R_o^3}{R^3}\right) - 4\mu\frac{\dot{R}}{R}. \tag{7}$$

In the limit $\lambda \to 0$ and $G \to 0$, the stress is purely viscous, such that the Keller-Miksis equation in a Newtonian fluid is recovered by substituting the strains from Eq. (3) into the stresses in Eq. (4), which themselves are then inserted into the bubble pressure Eq. (2).

Equations (1)–(2) and (6)–(7) form a closed system of three coupled nonlinear ordinary differential equations that describe the compressible dynamics of a spherical bubble in a linear viscoelastic medium exhibiting viscosity, elasticity, and stress relaxation. The present modeling approach extends other past studies of bubble dynamics in tissue, in which elasticity was neglected,[21,27] compressibility ignored,[21] and relaxation omitted.[25]

E. The final non-dimensional equations

The Keller-Miksis can then be written in non-dimensional form

$$\left(1 - \frac{\dot{R}}{C}\right)R\ddot{R} + \frac{3}{2}\left(1 - \frac{1}{3}\frac{\dot{R}}{C}\right)\dot{R}^2 = \left(1 + \frac{\dot{R}}{C}\right)\left[\left(1 + \frac{2}{We}\right)\frac{1}{R^{3\gamma}} - \frac{2}{WeR} + 3\varsigma - 1 - p_R\right]$$
$$-\frac{\dot{R}}{C}\left[\left(1 + \frac{2}{We}\right)\frac{3\gamma}{R^{3\gamma}} - \frac{2}{WeR}\right] + 3\frac{R}{C}\dot{\varsigma}, \tag{8}$$

with constitutive relations

$$De\dot{\tau}_{rr}|_R + \tau_{rr}|_R = -\frac{4}{3Ca}\left(1 - \frac{1}{R^3}\right) - \frac{4}{Re}\frac{\dot{R}}{R}, \tag{9}$$

$$De\dot{\varsigma} + \varsigma + De\frac{\dot{R}}{R}\tau_{rr}|_R = -\frac{4}{9Ca}\left(1 - \frac{1}{R^3}\right) - \frac{4}{3Re}\frac{\dot{R}}{R}, \tag{10}$$

and $De/Ca < 1/Re$.

Given that $Re = 3.0$ is constant, the ratio De/Ca can never be greater than 0.33. For $De = 0$ (Kelvin-Voigt or Newtonian models), there is no need to solve Eqs. (9) and (10). In light of the subsequent analysis, it is expected that De/Ca is a key parameter. This coupling can be made more evident by writing the stresses as

$$\tau_{rr}|_R = \tau_e + \tau_m, \qquad \text{where } \tau_e = -\frac{4}{3Ca}\left(1 - \frac{1}{R^3}\right), \tag{11}$$

$$\varsigma = \varsigma_e + \varsigma_m, \qquad \text{where } \varsigma_e = -\frac{4}{9Ca}\left(1 - \frac{1}{R^3}\right), \tag{12}$$

where e stands for elasticity and m for Maxwell, since without elasticity the Maxwell model is recovered. With this new definition of the stresses, the constitutive relations become

$$De\dot{\tau}_m + \tau_m = 4\frac{De}{Ca}\frac{\dot{R}}{R^4} - \frac{4}{Re}\frac{\dot{R}}{R}, \tag{13}$$

$$De\dot{\varsigma}_m + \varsigma_m + De\frac{\dot{R}}{R}\tau_m = \frac{4}{3}\left(\frac{De}{Ca} - \frac{1}{Re}\right)\frac{\dot{R}}{R}. \tag{14}$$

III. ANALYSIS AND RESULTS

Equations (8)–(10) constitute the system that is integrated numerically, and Eqs. (8), (13), and (14) form the basis for the analysis. All of the results have a non-dimensional pressure ratio of $p_R = 34$ and sound speed $C = 160$, Weber number $We = 9.0$ and Reynolds number $Re = 3.0$, unless otherwise stated.

A. Numerical solution to the equations

Exact solutions to the Rayleigh-Plesset and Keller-Miksis equations are generally difficult to obtain. Instead, a numerical solution to the system of equations (8)–(10) is obtained using a fifth-order accurate Cash-Karp Runge-Kutta method with adaptive stepsize control[48] to precisely capture violent bubble collapse by dynamically adjusting the time step. The equations can readily be solved numerically for a wide range of parameters. Sample numerical results are shown in this section to highlight important features of the bubble response specifically regarding elasticity, relaxation, and compressibility, which are explained in Sec. III B.

First, the dependence of the bubble dynamics on elasticity is shown in Fig. 2. Due to the problem setup and the final stress state, the final equilibrium radius increases with elasticity. One might expect that increasing the elasticity restricts the oscillations and therefore amplifies the damping. This behavior is indeed observed when comparing the solutions with the largest and intermediate elasticities, as the damping is higher and oscillation amplitude smaller for the case with larger G (i.e., smallest Ca). However, a counter-intuitive feature is observed as elasticity is decreased further: the oscillations for the case with lowest elasticity have higher damping, leading to a non-monotonic behavior of damping with elasticity. This observation can be quantified by considering the time elapsed at each rebound (Fig. 2, right): the intermediate elasticity exhibits the longest rebounds, such that the bubble dynamics persist for a longer time.

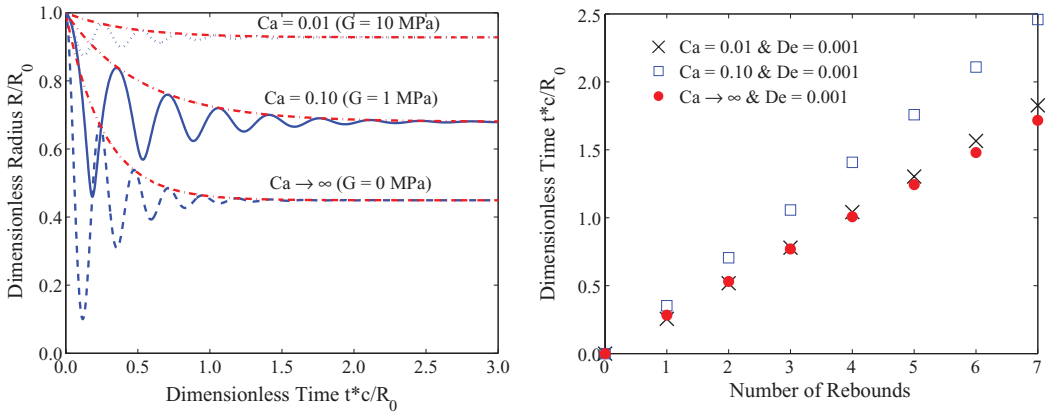

FIG. 2. Numerical solutions showing the dependence of the bubble oscillations on elasticity ($De = 0.001$, $p_R = 34$, $C = 160$, and $Re = 3.0$). (Left) History of the bubble radius: $Ca \to \infty$ (Maxwell; dashed), $Ca = 0.10$ (solid), and $Ca = 0.01$ (dotted); decay curves (dashed-dotted). (Right) Time to achieve a given rebound number: $Ca \to \infty$ (Maxwell; dots), $Ca = 0.10$ (circles), and $Ca = 0.01$ (crosses).

Next, the dependence of the bubble dynamics on relaxation is illustrated in Fig. 3. In this case, the equilibrium radius remains constant with *De*. The oscillation period and damping decrease with increasing Deborah number, consistent with past findings.[10] Although difficult to discern here, the frequency varies with time, first increasing before reaching a steady state. This behavior is not completely unexpected, due to the nonlinearity of the system, and will be confirmed through analysis.

Finally, the dependence of the bubble dynamics on compressibility and viscosity is highlighted in Fig. 4. The two main modes of damping are expected to be compressible and viscous. At high elasticity (small *Ca*), compressibility has a significant effect and dominates the damping (Fig. 4, left). On the other hand, at low elasticity (large *Ca*), viscous effects become more important (Fig. 4, right).

B. Multiple scales perturbation analysis

To explain the physics underlying the phenomena observed above and give a quantitative estimate of the oscillations behavior in general, the system of equations (8), (13), and (14) is analyzed. Although a linear perturbation analysis is expected to yield accurate results for small-amplitude and weakly nonlinear oscillations, it cannot capture the frequency-amplitude interaction

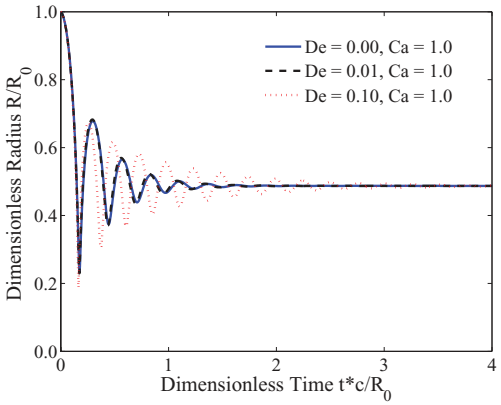

FIG. 3. Numerical solutions showing the history of the bubble radius for different relaxation times ($Ca = 1.0$, $p_R = 34$, $C = 160$, and $Re = 3.0$): $De = 0.00$ (Kelvin-Voigt; solid), $De = 0.01$ (dashed), and $De = 0.10$ (dotted).

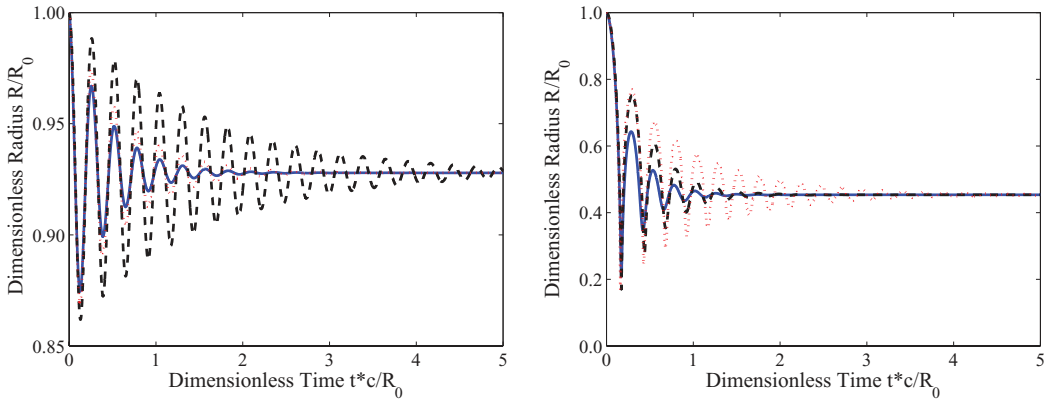

FIG. 4. Effects of the compressibility and viscosity at a fixed Ca ($p_R = 34$ and $De = 0$). (Left) History of the bubble radius at $Ca = 0.01$. (Right) History of bubble radius at $Ca = 10$. Numerical results with $C = 160$ and $Re = 3.0$ (compressible and viscous: solid), $C \to \infty$ and $Re = 3.0$ (incompressible and viscous: dashed), and $C = 160$ and $Re \to \infty$ (compressible and inviscid: dotted).

of highly nonlinear systems,[49] thus requiring a higher-order approach. Here, the multiple scales perturbation method is used, valid since the bubble oscillates about an equilibrium radius smaller than its initial value. The idea is to expand the radius as a function of several independent scales instead of a single one.[50] The Rayleigh-Plesset equation has been studied previously using this method, but not with the present setup or constitutive models.[21,22,51–53] In another approach, Prosperetti[54,55] used the method of averaging to examine the transient and steady-state response of a bubble. All of these studies were based on small-amplitude harmonic forcing in Newtonian or Maxwell fluids and hence oscillations about the initial (equilibrium) radius.

The governing equations are written into a first-order system, $\dot{\mathbf{x}} = \mathbf{f}(\mathbf{x})$, where $\mathbf{x} = (R, \dot{R}, \tau_m, \varsigma_m)^T$. There exists only one equilibrium point $\mathbf{x_0} = (R_f, 0, 0, 0)^T$ for this system, where the final equilibrium radius R_f is obtained through the following equation:

$$\left(1 + \frac{2}{We}\right)\frac{1}{{R_f}^{3\gamma}} - \frac{2}{WeR_f} + \tau_{e,f} - p_R - 1 = 0, \qquad \text{where } \tau_{e,f} = -\frac{4}{3Ca}\left(1 - \frac{1}{R_f^3}\right). \quad (15)$$

Thus, for a given gas and surface tension, R_f is a function of the amplitude of the driving pressure and elasticity, but does not depend on compressibility, viscosity, or relaxation. As shown in Fig. 5, R_f increases with increasing elasticity. This behavior is not surprising since a stiffer material (higher

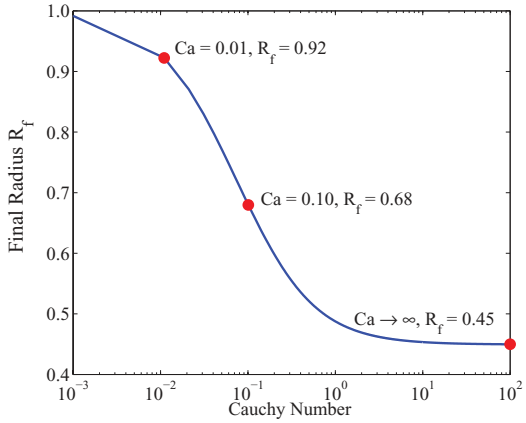

FIG. 5. Final (equilibrium) radius R_f as a function of elasticity ($De = 0.001$, $p_R = 34$, $C = 160$, and $Re = 3.0$). The dots correspond to the Cauchy numbers under consideration in Fig. 2.

elasticity) is expected to exhibit a lesser response to a given pressure change. Since the bubble and surrounding medium, initially in mechanical equilibrium, are subjected to a step increase in pressure, the final stress state has been increased by p_R from the initial state in this Rayleigh collapse, thus leading to a smaller final radius R_f. It follows that the equilibrium radius for the Maxwell component of the stress is zero. In the limit $G \to 0$, Eq. (15) reduces to the classical result.[13]

The Jacobian matrix of the first-order system is evaluated at the equilibrium point $\mathbf{A} = \nabla \mathbf{f}(\mathbf{x_0})$ to obtain the eigenvalues

$$(De\lambda + 1)\left\{De\lambda^3 + \left[1 + \frac{\omega_N^2 R_f De}{C} + \frac{4}{CR_f}\left(\frac{1}{Re} - \frac{De}{Ca}\right)\right]\lambda^2 + \left[\omega_N^2\left(\frac{R_f}{C} - De\right) + \frac{4}{R_f^2}\left(\frac{1}{Re} - \frac{De}{Ca}\right)\right]\lambda + \omega_N^2\right\} = 0, \tag{16}$$

where

$$\omega_N = \frac{1}{R_f}\sqrt{\left(1 + \frac{2}{We}\right)\frac{3\gamma}{R_f^{3\gamma}} - \frac{2}{WeR_f} + \frac{4}{CaR_f^3}} \tag{17}$$

is the bubble natural frequency. Compared to the standard result (e.g., Minnaert[56] frequency), an extra term accounting for elasticity is added. The elasticity affects the natural frequency explicitly through Ca and implicitly through R_f, such that the overall effect is not trivial. The inclusion of the two additional differential equations for the stresses due to relaxation complicates the solution by adding two eigenvalues. Clearly, one is $-1/De$. In the cubic polynomial, there is one real negative root and two complex roots; the real part of the complex roots are found to be negative numerically provided $De/Ca < 1/Re$, which means the nonlinear system is always asymptotically stable in the physically allowable regime.

When $De \ll 1/Re$, the time derivative of stresses in Eqs. (9) and (10) is negligible compared to the rest of the terms. A linear analysis is sufficient to obtain the asymptotic solution. As De increases, due to the strong coupling between the governing equation and constitutive relations, the full system becomes highly nonlinear and a simple linear analysis fails. Fig. 6 shows the failure of the linear theory by comparing such an approach with the corresponding numerical solution. Clearly, both the frequency and damping coefficient obtained from the linear analysis are incorrect. In nonlinear systems, the amplitude and phase of the oscillations may depend upon each other.[49] As a result, the frequency may vary with time, such that higher-order terms in the perturbation analysis are required. Such shifts in the frequency build up over time and lead to significant discrepancies.

The method of multiple scales[50] produces an approximate solution that captures the time-varying frequency and agrees well with the numerical solution. First, the solution is expanded about

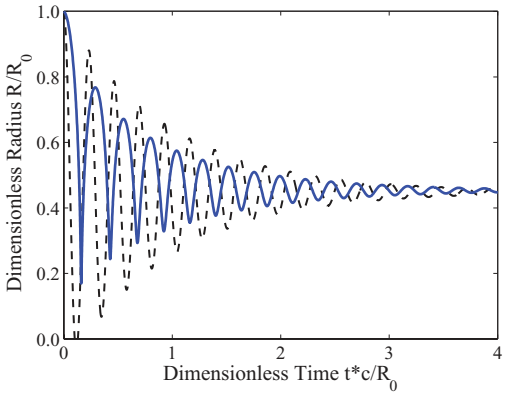

FIG. 6. Failure of the linear analysis for the Zener model ($De = 1$, $Ca = 101$, $p_R = 34$, $C = 160$, and $Re = 3.0$): numerical results (solid), linear perturbation analysis (dashed).

the (final) equilibrium conditions,

$$R(t) = R_f + x(t), \qquad \tau_m = \tau_{m,f} + y(t), \qquad \varsigma_m = \varsigma_{m,f} + z(t). \tag{18}$$

Since Eq. (15) is the only equilibrium point of the system, $\tau_{m,f}$ and $\varsigma_{m,f}$ are zero. The equations for x, y, and z yield, up to third order

$$\ddot{x} + \beta\dot{x} + \omega_N^2 x = f_1(x, \dot{x}, z, \dot{z}), \qquad \dot{y} + \frac{1}{De}y = f_2(x, \dot{x}), \qquad \dot{z} + \frac{1}{De}z = f_3(x, \dot{x}, y), \tag{19}$$

where ω_N is given in Eq. (17) and β is defined as

$$\beta = \frac{\omega_N^2 R_f}{C} + \frac{4}{C R_f De}\left(\frac{1}{Re} - \frac{De}{Ca}\right) \tag{20}$$

and f_1, f_2, and f_3 are given as

$$\begin{aligned} f_1 \;=& -\frac{3}{2R_f}\dot{x}^2 - \frac{2\omega_N^2}{C}x\dot{x} + \alpha_1 x^2 - \frac{R_f\omega_N^2}{C^2}\dot{x}^2 + \frac{\beta_2}{C}x\dot{x} + \frac{3}{2R_f^2}x\dot{x}^2 - \frac{1}{R_f C}\dot{x}^3 + \frac{2\alpha_1}{C}\dot{x}x^2 + \alpha_2 x^3 \\ & - \frac{2\omega_N^2}{C^2}x\dot{x}^2 - \frac{\omega_N^2}{C^3}\dot{x}^3 + \frac{\beta_3}{C^2}x\dot{x}^2 + \frac{\beta_4}{C}\dot{x}x^2 + \frac{3}{R_f}z + \frac{3}{C}\dot{z} - \frac{3}{R_f^2}xz + \frac{6}{R_f C}\dot{x}z + \frac{6}{R_f C^2}\dot{x}^2 z \\ & + \frac{3}{C^2}\dot{x}\dot{z} + \frac{3}{R_f^3}x^2 z - \frac{6}{R_f^2 C}x\dot{x}z + \frac{3}{C^3}\dot{x}^2\dot{z}, \end{aligned} \tag{21a}$$

$$f_2 \;= 4\left(\frac{1}{CaR_f^3} - \frac{1}{ReDe}\right)\frac{\dot{x}}{R_f} - 4\left(\frac{4}{CaR_f^3} - \frac{1}{ReDe}\right)\frac{x\dot{x}}{R_f^2} + 4\left(\frac{10}{CaR_f^3} - \frac{1}{ReDe}\right)\frac{x^2\dot{x}}{R_f^3}, \tag{21b}$$

$$f_3 \;= -\frac{\dot{x}y}{R_f} + \frac{x\dot{x}y}{R_f^2} + \frac{4}{3}\left(\frac{1}{Ca} - \frac{1}{ReDe}\right)\frac{\dot{x}}{R_f} - \frac{4}{3}\left(\frac{3}{4Ca} - \frac{1}{ReDe}\right)\frac{x\dot{x}}{R_f^2} + \frac{4}{3}\left(\frac{1}{Ca} - \frac{1}{ReDe}\right)\frac{x^2\dot{x}}{R_f^3}. \tag{21c}$$

The terms with β_3 and β_4 end up being neglected based on subsequent assumptions. The constants in the functions f_1, f_2, and f_3 are

$$\alpha_1 = \frac{1}{R_f^3}\left[\frac{9\gamma(\gamma+1)}{2}\left(1 + \frac{2}{We}\right)\frac{1}{R_f^{3\gamma}} - \frac{4}{WeR_f} + \frac{12}{CaR_f^3}\right], \tag{22a}$$

$$\alpha_2 = \frac{1}{R_f^4}\left[-\frac{9\gamma^2 + 18\gamma + 11}{2}\left(1 + \frac{2}{We}\right)\frac{1}{R_f^{3\gamma}} + \frac{6}{WeR_f} - \frac{76}{3CaR_f^3}\right], \tag{22b}$$

$$\beta_2 = \frac{4}{3}\frac{1}{R_f^2 Ca}\left(1 + \frac{8}{R_f^3}\right). \tag{22c}$$

Next, the small parameter ϵ is defined: $x = \epsilon u$, $y = \epsilon v$, and $z = \epsilon w$, which directly implies $y, z \sim O(\epsilon^2)$. To facilitate the analysis, two additional assumptions are made: $1/Re \sim \epsilon$, and $1/C \sim \epsilon^2$. Equivalently, y and z are of order $\dot{x}/Re, \dot{x}De/Ca$, a result that will be used later. The Reynolds number assumption allows the stresses to be carried over to the higher-order equations, and the sound speed assumption permits the simplification of certain higher-order terms. These assumptions are discussed in greater detail in Sec. III B 4. For the parameter range of interest, these assumptions are good, as validated by the results. From the model constraint $De/Ca < 1/Re$, $De/Ca \sim O(\epsilon)$ or less, such that the terms involving De/Ca and $1/Re$ are second order at the earliest. Equation (19) can then be re-written

$$\ddot{u} + \omega_N^2 u = \epsilon\left(\alpha_1 u^2 - \frac{3}{2R_f}\dot{u}^2 + \frac{3}{R_f}z\right) + \epsilon^2\left(-\beta_1\dot{u} + \alpha_2 u^3 + \frac{3}{2{R_f}^2}u\dot{u}^2 - \frac{3}{{R_f}^2}uz\right), \tag{23}$$

where $\beta \to \beta_1$ for small $1/ReDe$, with

$$\beta_1 = \frac{\omega_N^2 R_f}{C} - \frac{4}{CaC R_f}. \tag{24}$$

According to the method of multiple scales, u is expanded as follows:

$$u(t) = u_0(T_0, T_1, T_2) + \epsilon u_1(T_0, T_1, T_2) + \epsilon^2 u_2(T_0, T_1, T_2), \tag{25}$$

where $T_n = \epsilon^n t$ for $n = 0, 1, 2$, and the appropriate derivatives are defined. Terms up to ϵ^2 are retained for u, i.e., R is expanded to order ϵ^3, and the stresses are treated accordingly. The first and second time derivatives are defined as

$$\frac{d}{dt} = \sum_{n=0} \epsilon^n D_n = D_0 + \epsilon D_1 + \epsilon^2 D_2, \tag{26}$$

$$\frac{d^2}{dt^2} = D_0^2 + 2\epsilon D_0 D_1 + \epsilon^2 (D_1^2 + 2 D_0 D_2), \tag{27}$$

where $D_n \triangleq \frac{\partial}{\partial T_n}$. The stresses are expanded in a fashion similar to u; only the leading term is required. After substituting Eq. (25) into Eq. (23), the same-order terms can be collected.

- For $O(\epsilon)$,

$$D_0^2 u_0 + \omega_N^2 u_0 = 0. \tag{28}$$

  Thus, u_0 is harmonic with no damping

$$u_0 = \mathcal{A}_0(T_1, T_2) \exp(i\omega_N T_0) + cc, \tag{29}$$

  where cc is the complex conjugate of the preceding term and $\mathcal{A}_0$ is a complex function that may depend on T_1 and T_2 in general. As seen below, $\mathcal{A}_0$ is calculated by requiring u_1 and u_2 to be periodic in T_0. To carry out the analysis appropriately, it is essential to keep this first-order equation in the form of Eq. (28).
- For $O(\epsilon^2)$,

$$\begin{aligned} D_0^2 u_1 + \omega_N^2 u_1 =& -2 D_0 D_1 u_0 + \alpha_1 u_0^2 - \frac{3}{2R_f}(D_0 u_0)^2 \\ =& -2i\omega_N D_1 \mathcal{A}_0 \exp(i\omega_N T_0) + \alpha_1 [\mathcal{A}_0^2 \exp(i 2\omega_N T_0) + \mathcal{A}_0 \bar{\mathcal{A}}_0] \\ & - \frac{3\omega_N^2}{2R_f} [\mathcal{A}_0 \bar{\mathcal{A}}_0 - \mathcal{A}_0^2 \exp(i 2\omega_N T_0)] + cc, \end{aligned} \tag{30}$$

  where $\bar{\mathcal{A}}_0$ denotes the complex conjugate of $\mathcal{A}_0$. This solution is obtained by substituting u_0 into Eq. (30). Any particular solution to the above equation has a secular term containing the factor $\exp(i\omega_N T_0)$ unless $D_1 \mathcal{A}_0 = 0$. Therefore, $\mathcal{A}_0$ must be independent of T_1, such that u_1 can be expressed as

$$\begin{aligned} u_1 &= \mathcal{A}_1 \exp(i\omega_N T_0) + \mathcal{B}_1 + cc, \\ \text{where } \mathcal{A}_1 &= -\frac{\mathcal{A}_0^2}{3}\left(\frac{\alpha_1}{\omega_N^2} + \frac{3}{2R_f}\right), \quad \mathcal{B}_1 = \mathcal{A}_0 \bar{\mathcal{A}}_0 \left(\frac{\alpha_1}{\omega_N^2} - \frac{3}{2R_f}\right). \end{aligned} \tag{31}$$

- For $O(\epsilon^3)$,

$$\begin{aligned} D_0^2 u_2 + \omega_N^2 u_2 =& -D_1^2 u_0 - 2 D_0 D_1 u_1 - 2 D_0 D_2 u_0 + \beta_1 D_0 u_0 + 2\alpha_1 u_0 u_1 \\ & - \frac{3}{R_f}(D_0 u_0)[(D_1 u_0) + (D_0 u_1)] + \alpha_2 u_0^3 + \frac{3}{2R_f^2} u_0 (D_0 u_0)^2 + \frac{3}{R_f} w_1 \end{aligned} \tag{32}$$

  and

$$D_0 w_1 + \frac{1}{De} w_1 = -\frac{4}{3 De Re R_f}(D_0 u_0 - \lambda D_0^2 u_0). \tag{33}$$

The solution to Eq. (33) can be written as

$$w_1 = (\mathcal{C}_{1r} + i\mathcal{C}_{1i})\mathcal{A}_0 \exp(i\omega_N T_0) + cc + \mathcal{D}_1(T_1, T_2)\exp(-T_0/De), \tag{34}$$

where

$$\mathcal{C}_{1r} = \frac{4}{3}\frac{1}{R_f}\left(\frac{De}{Ca} - \frac{1}{ReR_f}\right)\frac{\omega_N^2 De}{1+\omega_N^2 De^2}, \qquad \mathcal{C}_{1i} = \frac{\mathcal{C}_{1r}}{\omega_N De}. \tag{35}$$

Substituting Eqs. (28), (30), and (34) into Eq. (32) yields

$$D_0^2 u_2 + \omega_N^2 u_2 = \mathcal{A}_2 \exp(i\omega_N T_0) + c_1 \mathcal{A}_0^3 \exp(3i\omega_N T_0) + cc + \frac{3\mathcal{D}_1}{R_f}\exp(-T_0/De), \tag{36}$$

where the coefficient of the secular term for u_2 is

$$\mathcal{A}_2 = -2i\omega_N(D_2\mathcal{A}_0) - \beta_1(i\omega_N)\mathcal{A}_0 + \frac{3}{R_f}(\mathcal{C}_{1r} + i\mathcal{C}_{1i})\mathcal{A}_0 + \mathcal{B}_2\mathcal{A}_0^2\bar{\mathcal{A}}_0, \tag{37}$$

with

$$\mathcal{B}_2 = 2\alpha_1\left(\frac{\mathcal{A}_1}{\mathcal{A}_0^2} + 2\frac{\mathcal{B}_1}{\mathcal{A}_0\bar{\mathcal{A}}_0}\right) + 3\alpha_2 + \frac{3\omega_N^2}{2R_f} - \frac{6\omega_N^2\mathcal{A}_1}{\mathcal{A}_0^2 R_f},$$

and c_1 is a constant of the higher order term. The secular term in Eq. (36) can be set to zero and separated into real and imaginary parts by introducing

$$\mathcal{A}_0 = \mathcal{A}_{0a}(T_2)\exp[i\mathcal{A}_{0\theta}(T_2)]. \tag{38}$$

The real and imaginary parts are given by the following differential equations:

$$\begin{aligned} -2\omega_N\frac{\partial\mathcal{A}_{0a}}{\partial T_2} + \left(-\beta_1\omega_N + \frac{3\mathcal{C}_{1i}}{R_f}\right)\mathcal{A}_{0a} = 0, \\ 2\omega_N\mathcal{A}_{0a}\frac{\partial\mathcal{A}_{0\theta}}{\partial T_2} + 3\mathcal{C}_{1r}\mathcal{A}_{0a} + \mathcal{B}_2\mathcal{A}_{0a}^3 = 0, \end{aligned} \tag{39}$$

whose solutions $\mathcal{A}_{oa}$ and $\mathcal{A}_{o\theta}$ are

$$\mathcal{A}_{0a} = \mathcal{F}_1\exp(\mathcal{E}_1 T_2), \qquad \mathcal{A}_{0\theta} = -\frac{3\mathcal{C}_{1r}}{2\omega_N}T_2 - \frac{\mathcal{B}_2\mathcal{F}_1^2}{4\mathcal{E}_1\omega_N}\exp(2\mathcal{E}_1 T_2) + \mathcal{F}_2, \tag{40}$$

where

$$\mathcal{E}_1 = -\frac{\beta_1}{2} + \frac{3\mathcal{C}_{1i}}{2\omega_N R_f}, \tag{41}$$

and $\mathcal{F}_1$ and $\mathcal{F}_2$ are constants determined by the initial conditions

$$R(0) = 1, \qquad \dot{R}(0) = -p_R/C. \tag{42}$$

1. Oscillations characteristics: Damping and frequency

From the above analysis, the leading term of the damping can be expressed as a linear combination of a compressible contribution β_c and a viscous component β_v

$$\beta_{tot} = \beta_c + \beta_v = \frac{R_f\omega_N^2}{2C} + \frac{2}{R_f}\left(\frac{1}{ReR_f} - \frac{De}{Ca}\right)\frac{1}{1+\omega_N^2 De^2}. \tag{43}$$

Both components depend on elasticity. However, relaxation only affects the viscous term weakly, and decreases monotonically with increasing Ca. The compressible component can be broken up into thermal, interfacial tension, and elastic contributions,[25] i.e.,

$$\beta_c = \frac{R_f\omega_N^2}{2C} = \left[\frac{3\gamma}{2}\left(1 + \frac{2}{We}\right)\frac{1}{R_f^{3\gamma}} - \frac{1}{WeR_f} + \frac{2}{CaR_f^3}\right]\frac{1}{R_f C}. \tag{44}$$

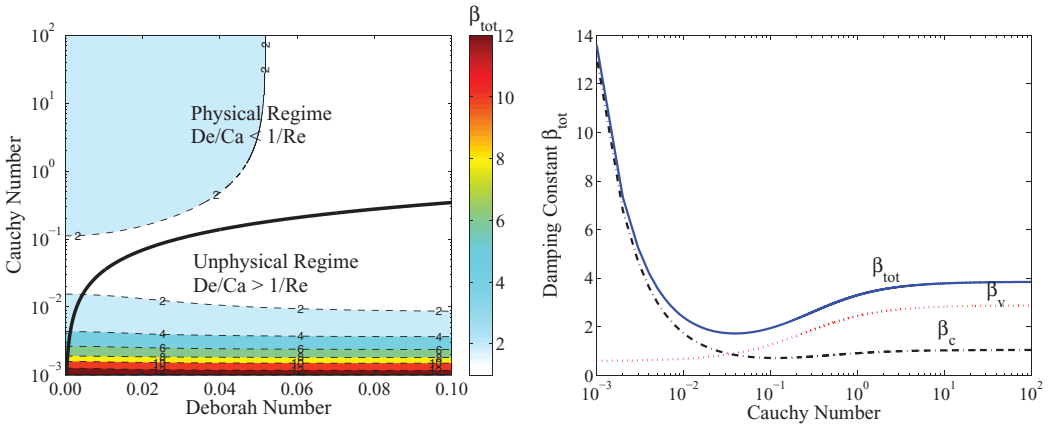

FIG. 7. Dependence of the damping coefficient on De and Ca ($p_R = 34$, $C = 160$, and $Re = 3.0$). The physical regime indicates that the constraint $De/Ca < 1/Re$ is met. (Left) Contour plots. (Right) Representative line plot holding $De = 0.001$ constant: β_{tot} (solid), β_v (dotted), β_c (dashed-dotted).

Although seemingly unstable, surface tension never dominates the thermal term. The damping in Eq. (44) acts only if compressibility is present. For sufficiently large Reynolds number, the viscous damping is negligible. Furthermore, due to the physical constraint between Re, De, and Ca, a large Reynolds implies a small relaxation time for a fixed elasticity, such that relaxation effects no longer matter, which is consistent with Brujan.[28] Equation (43) only includes first-order effects; higher-order terms are needed to represent the damping accurately, but cannot be written as readily.

The dependence of the damping coefficient Eq. (43) on Ca and De is shown in Fig. 7. The boundary of the model constraint ($De/Ca < 1/Re$) is highlighted by a line, to show the physically appropriate phase space region. For a fixed Ca, the damping decreases monotonically with increasing De. For a fixed De, the damping is non-monotonic with respect to Ca (Fig. 7). As expected, the viscous and compressible components add up to the total damping. These observations offer a quantitative explanation of the behavior shown in Fig. 4. Specifically, at small Ca (large elasticity), β_c dominates the damping, as expected from the constitutive relation where the viscous contribution becomes negligible. At higher Ca (smaller elasticity), β_v becomes more important than compressibility. The viscous term of the damping coefficient increases with decreasing elasticity (i.e., as Ca increases), while the compressibility component follows the inverse trend, i.e., β_c decreases with increasing Cauchy number, since R_f is bounded; this is expected given that R_f decreases with decreasing elasticity (Fig. 5). Since the compressible component decreases before the viscous term increases (as a function of Ca), the damping coefficient has a minimum for a finite non-zero elasticity, which falls in the range of reported tissue elasticities.[25] This result explains why the intermediate value of Ca results in less damping in Fig. 2.

The oscillatory component of the solution consists of simple harmonic motion and a time-dependent term that decays exponentially with time, as observed in the leading term

$$\exp\left\{i\omega_N\left[T_0 + \frac{2}{R_f}\left(\frac{1}{ReR_f} - \frac{De}{Ca}\right)\frac{De}{1+\omega_N^2 De^2}T_2 - \frac{\mathcal{F}_1^2}{4\mathcal{E}_1\omega_N^2}\mathcal{B}_2(T_2)\exp(2\mathcal{E}_1 T_2)\right]\right\}. \tag{45}$$

The multiple scales analysis adds two terms that depend on relaxation to the frequency obtained from linear analysis: a constant and an exponential decay ($\mathcal{E}_1 < 0$). For small De, the interaction between frequency and amplitude (nonlinearity) is weak; as De approaches zero, the frequency from the linear solution is recovered. The first additional term in Eq. (45), small in the cases of interest, simply indicates that bubbles oscillate faster when relaxation is present. The second additional term is time-dependent and introduces relaxation, i.e., the time it takes for the surroundings to recover. It takes a few cycles for the frequency to reach a steady-state value, in which case the frequency goes

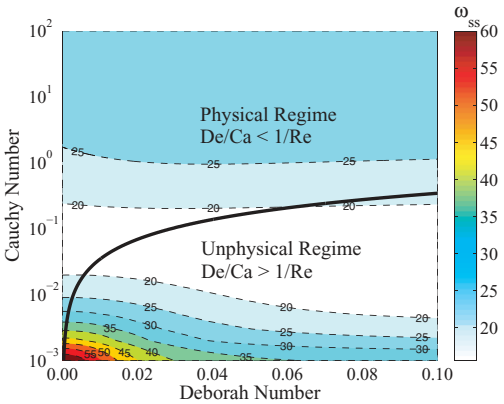

FIG. 8. Frequency at the steady state as a function of De and Ca ($p_R = 34$, $C = 160$, and $Re = 3.0$). The physical regime indicates that the constraint $De/Ca < 1/Re$ is met.

as

$$\omega_{ss} = \omega_N + \frac{\omega_N De}{1 + \omega_N^2 De^2} \frac{2}{R_f} \left(\frac{1}{ReR_f} - \frac{De}{Ca} \right). \tag{46}$$

The dependence of ω_{ss} on Ca and De is shown in Figs. 8 and 9. The dependence on Ca is strong and, similarly to β, non-monotonic. Viscosity and compressibility weakly affect ω_{ss}. The minimum is also due to the dependence of the equilibrium radius on the elasticity in Eq. (15). There is always a maximum in the graph of frequency as a function of De, as expected from Eq. (45). However, the ω_{ss} variations with De are relatively small.

To assess the accuracy of the analysis, Fig. 10 provides a comparison between the numerical solution and the multiple scales results for the Zener model with various De and Ca. The damping, time-dependent frequency (Fig. 6) and nonlinearities are well captured, thus validating this approach. Furthermore, it is clear that the present third-order expansion is required to represent the time-varying oscillation period, and that the assumptions made during the analysis are valid. Subharmonics appear in the analytical result at the peaks. The predicted frequency clearly increases with time.

In summary, the method of multiple scales has been used successfully to provide an analytical solution for the oscillations of a bubble in a Zener viscoelastic medium. Equations (43) and (45) give a good approximation of the damping and frequency, thus providing accurate predictions of bubble oscillations for known viscoelastic properties, which can be useful in a biomedical setting, e.g., to

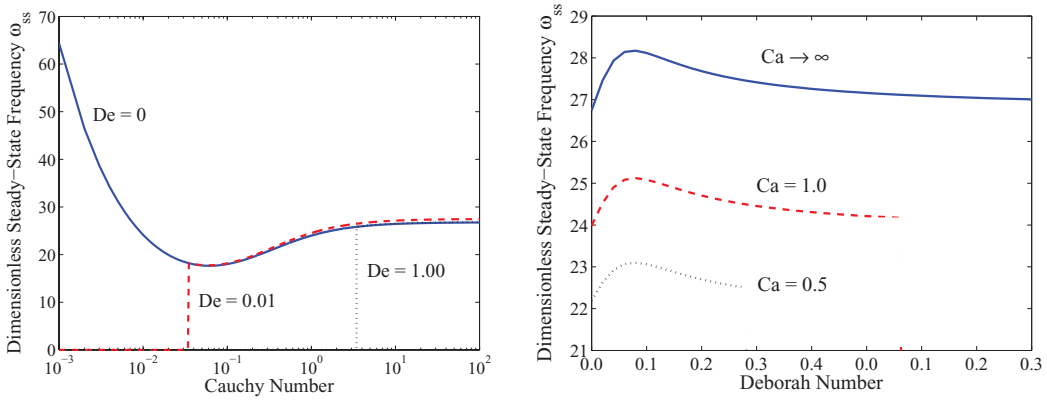

FIG. 9. Dependence of the frequency at the steady state on De and Ca independently ($p_R = 34$, $C = 160$, and $Re = 3.0$). (Left) ω_{ss} vs. Ca. $De = 0$ (Kelvin-Voigt; solid), $De = 0.01$ (dashed), $De = 1$ (dotted). (Right) ω_{ss} vs. De. $Ca \to \infty$ (Maxwell; solid), $Ca = 1$ (dashed), $Ca = 0.5$ (dotted).

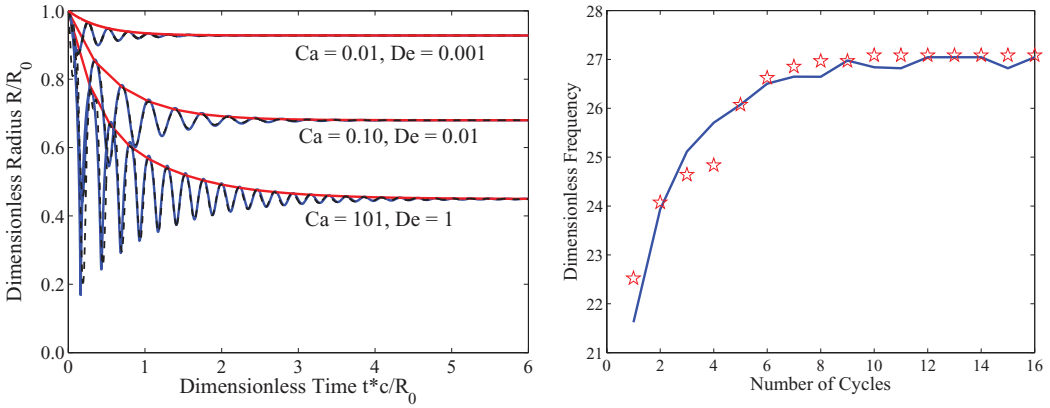

FIG. 10. Validation of the theoretical results against the numerical solution ($p_R = 34$, $C = 160$, and $Re = 3.0$). (Left) History of the bubble radius for different Ca and De. From top to bottom: $Ca = 0.01$ and $De = 0.001$, $Ca = 0.10$ and $De = 0.01$, and $Ca \to \infty$ and $De = 1$ (Maxwell); thick solid: numerical solution; dashed: multiple scales; thin solid: decay curve. (Right) Frequency at the steady state vs. number of cycles for a single run with the Zener model ($De = 1$, $Ca = 101$). Numerical solution: solid; theory: stars.

determine how long bubbles oscillate in a given application. The restrictions of the present analysis lie in the assumptions that $1/Re$ and $1/C$ both be small (order ϵ). While the mathematical approach is sound even for large-amplitude oscillations, a linear constitutive model may not be appropriate for large strains.

2. Collapse properties: Minimum radius and collapse time

The minimum radius, achieved at the first collapse, is an important quantity with respect to potential damage caused by bubble collapse, since it directly relates to the maximum pressure (for an adiabatic process, $pR^{3\gamma} = \text{constant}$) and thus shock emission. From this quantity, one can compute the collapse time, which can readily be measured acoustically in experiments. Two approaches are followed to predict the minimum radius and the collapse time: one based on direct integration of the Rayleigh-Plesset equation (with no compressibility), and one based on the linear analysis for the Keller-Miksis equation. To simplify the analysis, $De = 0$ in this section.

Direct integration of Eq. (1) for the Rayleigh collapse problem can be done by setting C, $Re \to \infty$ (incompressible and inviscid).[13] While restrictive, these assumptions are still expected to produce a reasonable result. Both compressibility and viscosity have their largest effect near collapse, and the time over which the high velocities are generated is short; since both effects depend on velocity, the collapse time is not expected to be affected significantly, though the minimum radius may be. The results confirm these hypotheses.

Since p_R is constant and $De = 0$, Eq. (1) can be integrated by multiplying through by $2R^2\dot{R}$ and forming appropriate time derivatives. After integration, application of the initial conditions $\dot{R}(0) = 0$ and $R(0) = 1$ yields the velocity of the bubble wall

$$\dot{R}^2 = \frac{2}{3(\gamma-1)}\left(1+\frac{2}{We}\right)\left(\frac{1}{R^3}-\frac{1}{R^{3\gamma}}\right) - \frac{2}{We}\left(\frac{1}{R}-\frac{1}{R^3}\right) - \frac{2}{3}\left(1+p_R+\frac{4}{3Ca}\right)\left(1-\frac{1}{R^3}\right) + \frac{8}{3Ca}\frac{\ln R}{R^3}, \tag{47}$$

which is equivalent to the result shown in Brennen,[13] with two additional terms for elasticity. The minimum bubble radius is obtained by setting $\dot{R} = 0$ above and solving for the corresponding radius R_{min}.

By re-arranging Eq. (47), it follows that

$$t_c = \int_1^{R_{min}} \left[\frac{2\left(1+\frac{2}{We}\right)}{3(1-\gamma)}(x^{-3\gamma} - x^{-3}) - \frac{2}{We}(x^{-1} - x^{-3}) - \zeta(1-x^{-3}) + \frac{8}{3Ca}\frac{\ln(x)}{x^3} \right]^{-1/2} dx, \tag{48}$$

where $\zeta = \frac{2}{3}(1 + p_R + \frac{4}{3Ca})$. This integral can be evaluated numerically to find the collapse time t_c since R_{min} is known.

The second approach is based on linear analysis, valid for sufficiently small oscillations. To first order,

$$R(t) = c_1 \exp(-\beta_{tot} t)\cos(\omega t) + c_2 \exp(-\beta_{tot} t)\sin(\omega t), \tag{49}$$

where $\omega = \sqrt{\beta_{tot}^2 - \omega_N^2}$. The collapse time is computed by setting the time derivative of the expression above to zero to obtain

$$t_c = \frac{1}{\beta - (1-R_f)\frac{\omega_N^2 C}{p_R}} + \frac{\pi}{\omega}. \tag{50}$$

This time is then substituted into the radius to obtain

$$R_{min} = R_f + e^{-\beta t_c}\left\{(1-R_f)\cos(\omega t_c) + \left[\frac{\beta}{\omega}(1-R_f) - \frac{p_R}{C\omega}\sin(\omega t_c)\right]\right\}. \tag{51}$$

The two approaches to predict the minimum radius and collapse time are compared to the numerical results with and without damping as a function of elasticity in Figs. 11 and 12. Since direct integration only holds in the limits C, $Re \to \infty$, the results from Eqs. (47) and (48) match the incompressible and inviscid solution very well. However, there is a discrepancy between the latter and the full compressible simulation. This discrepancy increases with smaller radius (here: with decreasing elasticity). Linear analysis account for both compressibility and viscosity, and thus matches the full simulation well as long as the oscillations are not too large, after which the solution deviates significantly. As explained above, the discrepancy for the collapse time is relatively small, but is larger for the minimum radius. The collapse time and minimum radius both clearly depend on elasticity, whose effect is to "soften" the collapse. While t_c exhibits non-monotonic behavior with Cauchy number consistent with the damping coefficient (Sec. III B 1), R_{min} decreases monotonically with increasing Cauchy number. Both of these quantities are important to biomedical applications, as they quantify the violence of the collapse.

The minimum radius can be used as a measure of nonlinearity of the bubble oscillation in this problem, e.g., as an *inertial cavitation threshold*.[15,16] For instance, the critical radius at which the

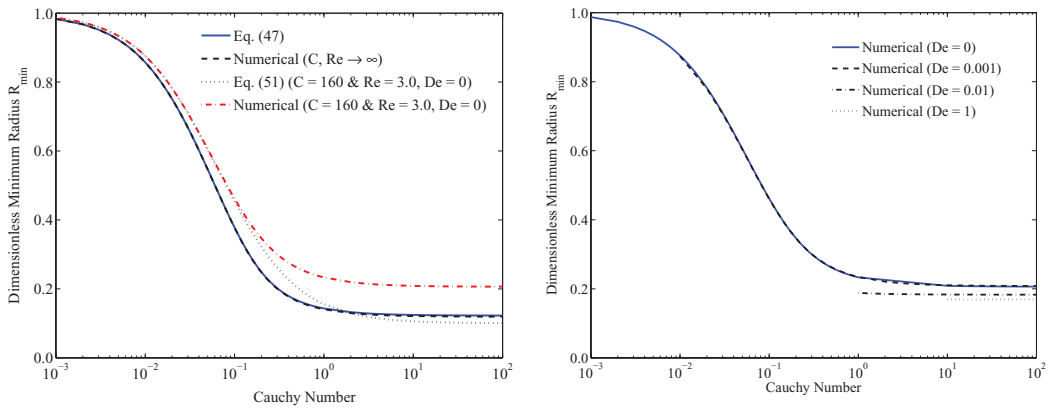

FIG. 11. Minimum radius at the first collapse as a function of elasticity ($p_R = 34$). (Left) Numerical results with $C = 160$ and $Re = 3.0$ (dashed-dotted); numerical results with $C \to \infty$ and $Re \to \infty$ (dashed); Eq. (47) with C, $Re \to \infty$ (solid); Eq. (51) with $C = 160$ and $Re = 3.0$ (dotted). (Right) Dependence on relaxation.

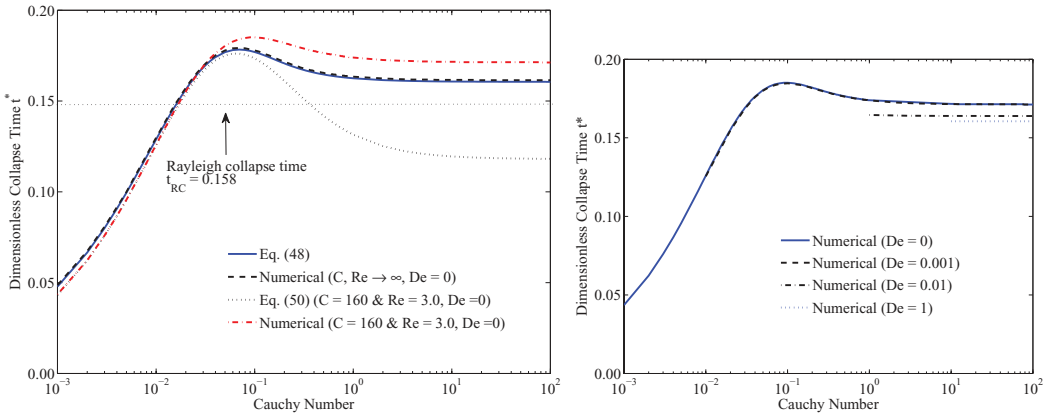

FIG. 12. Collapse time (for the first collapse) as a function of elasticity ($p_R = 34$). (Left) Numerical results with $C = 160$ and $Re = 3.0$ (dashed-dotted); numerical results with $C \to \infty$ and $Re \to \infty$ (dashed); Eq. (48) with C, $Re \to \infty$ (solid); Eq. (50) with $C = 160$ and $Re = 3.0$ (dotted). (Right) Dependence on relaxation.

linear solution deviates from the full solution can be used to define the region in which linear analysis is expected to be accurate. Here, it appears that such a critical radius is $R \sim 0.5$. In other words, if $R_{min} \gtrsim 0.5$, one expects linear analysis to hold, and if $R_{min} \lesssim 0.5$, a more sophisticated approach, e.g., multiple scales, is required.

3. Special cases: Kelvin-Voigt and Maxwell models

Since Kelvin-Voigt and Maxwell models are arguably the simplest viscoelastic models, they are briefly discussed here. To get an appreciation for the differences with the Zener model, Fig. 13 compares these three models by considering the numerical solution.

In the limit $De \to 0$, the Kelvin-Voigt model is recovered. In this case, the constitutive relation no longer takes the form of two differential equations, such that simple linear perturbation analysis describes the solution very well for all Ca. The first-order equation simply takes the form of a damped harmonic oscillator with the bubble natural frequency and damping coefficient

$$\omega_N = \frac{1}{R_f}\sqrt{\frac{\left(1+\frac{2}{We}\right)\frac{3\gamma}{R_f^{3\gamma}} - \frac{2}{WeR_f} + \frac{4}{CaR_f^3}}{1+\frac{4}{ReCR_f}}}, \qquad \beta_{tot} = \frac{R_f\omega_N^2}{2C} + \frac{2}{R_f}\frac{1}{\left(ReR_f + \frac{4}{C}\right)}. \tag{52}$$

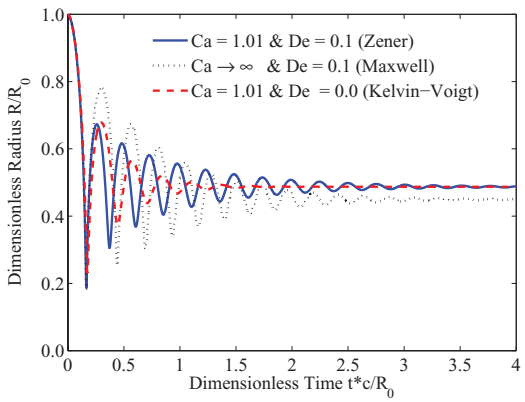

FIG. 13. History of the bubble radius for different constitutive models ($p_R = 34$, $C = 160$, and $Re = 3.0$). Solid: Zener ($Ca = 1.01$ and $De = 0.1$); dotted: Maxwell ($Ca = 0.0$ and $De = 0.1$); dashed: Kelvin-Voigt ($Ca = 1.01$ and $De = 0.0$).

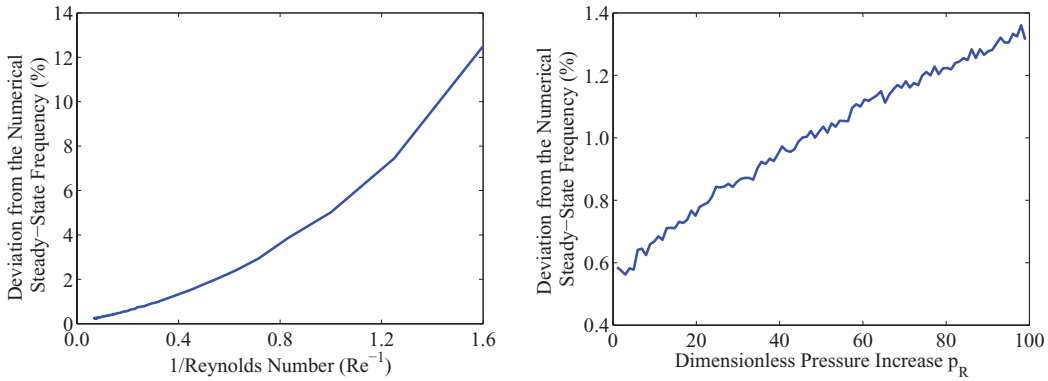

FIG. 14. Error in the steady-state frequency. (Left) Dependence on Reynolds number ($Ca = 0.10$, $De = 0.01$, and $p_R = 34$). (Right) Dependence on pressure amplitude ($Ca = 0.10$, $De = 0.01$, and $Re = 3.0$).

If $\beta_{tot}^2 < \omega_N^2$, the solution is oscillatory at frequency $\omega = \sqrt{\beta_{tot}^2 - \omega_N^2}$ with damping coefficient β_{tot}. If $\beta_{tot}^2 > \omega_N^2$, the system is overdamped, i.e., no oscillations occur. The corrections due to the coupling between viscous and compressible effects are readily included here. They are not present in the multiple scales analysis because of the Reynolds number assumption. Overall, the damping occurs more rapidly in Kelvin-Voigt than Zener for a fixed Ca (Fig. 13).

In the limit $Ca \to \infty$, the Maxwell model is recovered, which results in larger oscillations (and more damping) for a fixed De (Fig. 13). Furthermore, the equilibrium radius is different since there is no elasticity. For this model, there is no constraint on De and Re. The multiple scales analysis is still required due to the nonlinearity of the system and the two additional ordinary differential equations for the stresses. Thus, Eqs. (43) and (45) still hold, but $Ca \to \infty$ and R_f is fixed.

4. Range of validity of the multiple scales analysis

Two key assumptions are made in the analysis: $1/Re \sim \epsilon$ and $1/C \sim \epsilon^2$; given that $C = 160$, the latter is not further discussed. Another assumption is that the oscillations are not too large, such that the dependence on p_R is of interest as well. As a measure of the validity of the present analysis, the discrepancy in the frequency achieved at steady-state ω_{ss} calculated from the analytical solution and the numerical solution is computed and shown in Fig. 14 as a function of both $1/Re$ and p_R. This quantity is relatively easy to compute (e.g., as opposed to the damping coefficient), can readily be used across the whole parameter range, and exhibits noticeable errors even for a small discrepancy. For fixed values of Ca and De, the error increases with pressure amplitude, but remains small ($\sim$1%) even at high driving pressures. In such situations, it is more likely that a linear constitutive model no longer holds.

The dependence of the error on the Reynolds number is much more dramatic. As the Reynolds number is decreased even by a little, the error grows significantly. However, for the present value of $Re = 3.0$ (based on the viscosity of blood and the characteristic time and size), the analysis agrees well with the numerical solution and the error is small ($\sim$1%) despite $1/Re$ not being exceedingly small, thus validating the assumption $1/Re \sim \epsilon$. Based on these results, it is evident that this analysis may not be accurate for much smaller bubbles or more viscous media. Given the scope of this work, the dependence of the error on the other parameters (surface tension, compressibility) is not relevant.

C. Cavitation-bubble collapse

As described in Sec. II A, Rayleigh collapse is usually set up by perturbing the ambient pressure p_∞ by a positive change p_A. This effect is $O(1)$ and thus affects the final radius R_f. Another means by which collapse is achieved is by increasing the equilibrium radius (i.e., decreasing the interior pressure), so that Eq. (1) is disturbed through the gas pressure term $\sim(R_o/R)^{3\gamma}$; this perturbation

affects all equations of order higher than $O(1)$. In practice, a nucleus or small bubble subjected to a transient tension would grow to some maximum radius. At that stage, the ambient pressure is essentially atmospheric, but the interior pressure is small, thus causing collapse. The resulting dynamics are different from those observed in Sec. III because the overall stress state is different. Since the surrounding pressure is atmospheric during the bubble collapse ($p_A = 0$), the bubble eventually recovers its equilibrium radius. Although not included here to prevent redundancies, the analysis holds with trivial corrections. It can be shown that the damping coefficient and frequency increase monotonically with increasing elasticity because the final radius no longer depends on elasticity. However, comparisons with the results above would be misleading, because the growth depends on the material properties, such that, for a prescribed tension, the maximum radius will be different for different properties, thus making comparisons for the collapse difficult. An additional time scale related to growth would be introduced, further complicating the problem.

IV. CONCLUSIONS

The objective of the present study is to understand the basic physics of bubble dynamics in soft tissue. Theoretical and numerical models are developed to investigate the Rayleigh collapse and subsequent oscillations of a spherical gas bubble in tissue-like medium. This material is assumed to follow a linear Zener viscoelastic model that includes viscosity, elasticity, and stress relaxation. In addition to numerical integration of the equations, the method of multiple scales is used to predict the bubble response, specifically with respect to elasticity and relaxation in conditions under which compressibility is a factor.

The theory accurately predicts the bubble response given the relevant constraints for the problem under consideration, and can thus be used to investigate the underlying physics. The main observation is that the viscoelastic properties and compressibility strongly affect the dynamics. The key specific results are summarized below:

- Due to the nonlinearity of the system of equations, a third-order expansion of the radius about the final radius is necessary in general to accurately represent the dynamics.
- The final equilibrium radius is a function of the elasticity because of the stress field in this problem setup (Rayleigh collapse). It does not depend on relaxation, viscosity, or compressibility.
- The damping consists of the sum of viscous and compressible terms that exhibit opposite behavior with varying elasticity: the viscous contribution increases with decreasing elasticity, while the compressible component decreases with decreasing elasticity. Thus, compressible damping dominates at large elasticity and viscous at low elasticity. Because of the different behavior of each component, the total damping does not monotonically decrease with decreasing elasticity, but has a minimum for a finite non-zero elasticity in a range corresponding to reported tissue elasticities.
- Relaxation affects the damping purely through the viscous component, which decreases monotonically with increasing relaxation time.
- Due to the nonlinearity of the system, the oscillation frequency changes with time: it first increases before reaching a plateau. This time-dependence can only be captured with a third-order expansion.
- The minimum radius and collapse time, both quantities of interest with respect to potential damage due to bubble collapse, can be predicted using two different approaches, for sufficiently small amplitudes. Deviations at larger amplitudes are purely due to either compressibility and viscous effects with the first approach, or amplitude size for the second. A criterion ($R_{min} \gtrsim 0.5$) is proposed for the range of validity of the linear analysis based on the predicted minimum radius.

The knowledge acquired in the present study may be useful for a variety of biomedical engineering applications that either rely on oscillating bubbles to achieve a given outcome or in which cavitation must be prevented, e.g., to determine how long bubbles keep oscillating and how violent a collapse is. The Zener model is arguably the simplest fluid and solid viscoelastic model, as it

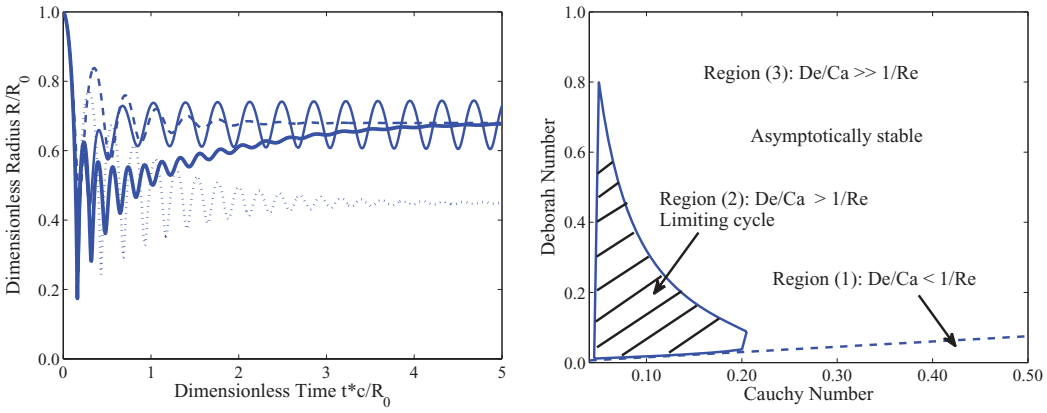

FIG. 15. History of the bubble radius for unphysical parameters in the Zener model ($De/Ca > 1/Re$, $p_R = 34$, $C = 160$, and $Re = 3.0$). (Left) $De/Ca = 0$ (Maxwell; dotted), $De/Ca = 1 > 1/Re$ (thin solid), $De/Ca = 10 \gg 1/Re$ (thick solid), $De/Ca = 0$ (Kelvin-Voigt; dashed). (Right) Marginal stability regions in phase space.

combines a Hookean solid with a Newtonian fluid. More sophisticated models for tissue include frequency-dependent coefficients, finite-strain analysis, and nonlinear viscoelasticity. Furthermore, large-amplitude oscillations are prone to non-spherical perturbation growth. To address these issues, current efforts focus on including more realistic constitutive relations (hyperelasticity, nonlinear viscoelasticity), and analytical (Rayleigh-Plesset extensions, non-spherical perturbation analysis) and computational (direct simulations of the full compressible equations of motion) methods.

APPENDIX: ADDITIONAL REMARKS ON CONSTITUTIVE MODELING

In Eq. (4), independent values of Re, De, and Ca may be selected, but a choice leading to $De/Ca > 1/Re$ produces a negative spring constant, which of course is unphysical. Nevertheless, the resulting behavior is interesting from a mathematical viewpoint. Fig. 15 (left) shows responses for various De that violate this constraint. When $De/Ca \gg 1/Re$, the solution lies between two limits: the solution initially follows the behavior in a purely Newtonian fluid before relaxing back to the Kelvin-Voigt solution; as De is decreased, the solution tends to the Kelvin-Voigt solution more rapidly. For these solutions, the oscillations eventually damp out. For $De/Ca \gtrsim 1/Re$, a boundary layer behavior is evident: after relaxing to the Kelvin-Voigt solution, the oscillations never decay beyond a certain point. Various time-marching schemes were used, such that this instability is unlikely to be numerical. The basic stability theorem states that if the linearized system is asymptotically stable, so is the full system. Thus, the original system is asymptotically stable outside the shaded region. If the linearized system is not asymptotically stable, the nonlinear terms in the original system must be investigated. In Eq. (16), the real part of the complex eigenvalue is positive for an intermediate range of De (region 2 in Fig. 15, right), which indicates that this region is not asymptotically stable. The curve of marginal stability is obtained by varying both Ca and De. As shown in Fig. 15 (right), the system is asymptotically stable outside the shaded region (regions 1 and 3) and unstable inside (region 2). For the unstable mode, instead of evolving in the unstable manifold, the steady-state solution is such that $R_{ss}(t) = R_{ss}(t + T)$ where T is the period of the oscillation. Thus, the dynamics converge to a limit cycle in the phase diagram, from which it is concluded that a Hopf bifurcation occurs when varying De. The solution never diverges, presumably due to the action of higher-order nonlinear terms.

[1] B. B. Goldberg, J. B. Liu, and F. Forsberg, "Ultrasound contrast agents: A review," Ultrasound Med. Biol. **20**, 319–333 (1994).
[2] J. E. Lingeman, "Extracorporeal shock wave lithotripsy: Development, instrument, and current status," Urol. Clin. North Am. **24**, 185–211 (1997).
[3] W. W. Roberts, T. L. Hall, K. Ives, J. S. Wolf, Jr., J. B. Fowlkes, and C. A. Cain, "Pulsed cavitational ultrasound: A noninvasive technology for controlled tissue ablation (histotripsy) in the rabbit kidney," J. Urol. **175**, 734–738 (2006).

[4] P. Hayward, "Traumatic brain injury: The signature of modern conflicts," Lancet Neurol. **7**, 200–201 (2008).
[5] E. Johnsen and T. Colonius, "Shock-induced collapse of a gas bubble in shockwave lithotripsy," J. Acoust. Soc. Am. **124**, 2011–2020 (2008).
[6] E. Johnsen and T. Colonius, "Numerical simulations of non-spherical bubble collapse," J. Fluid Mech. **629**, 231–262 (2009).
[7] A. R. Jamaluddin, G. J. Ball, C. K. Turangan, and T. G. Leighton, "The collapse of single bubbles and approximation of the far-field acoustic emissions for cavitation induced by shock wave lithotripsy," J. Fluid Mech. **677**, 305–341 (2011).
[8] C. Kim, "Collapse of spherical bubbles in maxwell fluids," J. Non-Newtonian Fluid Mech. **55**, 37–58 (1994).
[9] J. B. Freund, "Shock-induced bubble jetting into a viscous fluid with application to tissue injury in shock-wave lithotripsy," J. Acoust. Soc. Am. **126**, 2746–2756 (2009).
[10] K. Foteinopoulou and M. Laso, "Numerical simulation of bubble dynamics in a Phan-Thien–Tanner liquid: Non-linear shape and size oscillatory response under periodic pressure," Ultrasonics **50**, 758–776 (2010).
[11] S. J. Lind and T. N. Phillips, "Spherical bubble collapse in viscoelastic fluids," J. Non-Newtonian Fluid Mech. **165**, 56–64 (2010).
[12] S. J. Lind and T. N. Phillips, "Bubble collapse in compressible fluids using a spectral element marker particle method. Part 2. Viscoelastic fluids," Int. J. Numer. Methods Fluids **71**, 1103–1130 (2013).
[13] C. E. Brennen, *Cavitation and Bubble Dynamics* (University Press, Oxford, 1995).
[14] M. S. Plesset and A. Prosperetti, "Bubble dynamics and cavitation," Annu. Rev. Fluid Mech. **9**, 145–185 (1977).
[15] H. G. Flynn, "Cavitation dynamics. I. A mathematical formulation," J. Acoust. Soc. Am. **57**, 1379–1396 (1975).
[16] H. G. Flynn, "Cavitation dynamics. II. Free pulsations and models for cavitation bubbles," J. Acoust. Soc. Am. **58**, 1160–70 (1975).
[17] H. Fogler and J. Goddard, "Collapse of spherical cavities in viscoelastic fluids," Phys. Fluids **13**, 1135–1141 (1970).
[18] D. H. Kaelble, "Cavitation in viscoelastic media," Trans. Soc. Rheol. **15**, 275–296 (1971).
[19] W. J. Yang and M. L. Lawson, "Bubble pulsation and cavitation in viscoelastic liquids," J. Appl. Phys. **45**, 754–758 (1974).
[20] S. K. Hara and W. R. Schowalter, "Dynamics of nonspherical bubbles surrounded by viscoelastic fluid," J. Non-Newtonian Fluid Mech. **14**, 249–264 (1984).
[21] J. Allen and R. Roy, "Dynamics of gas bubbles in viscoelastic fluids. I. Linear viscoelasticity," J. Acoust. Soc. Am. **107**, 3167–3178 (2000).
[22] J. Allen and R. Roy, "Dynamics of gas bubbles in viscoelastic fluids. II. Nonlinear viscoelasticity," J. Acoust. Soc. Am. **108**, 1640–1650 (2000).
[23] D. Khismatullin and A. Nadim, "Radial oscillations of encapsulated microbubbles in viscoelastic liquids," Phys. Fluids **14**, 3534–3557 (2002).
[24] J. Jimenez-Fernandez and A. Crespo, "Bubble oscillation and inertial cavitation in viscoelastic fluids," Ultrasonics **43**, 643–651 (2005).
[25] X. Yang and C. Church, "A model for the dynamics of gas bubbles in soft tissue," J. Acoust. Soc. Am. **118**, 3595–3606 (2005).
[26] B. Patterson, D. L. Miller, and E. Johnsen, "Theoretical microbubble dynamics in a viscoelastic medium at capillary breaching thresholds," J. Acoust. Soc. Am. **132**, 3770–3777 (2012).
[27] E. A. Brujan, "A first-order model for bubble dynamics in a compressible viscoelastic liquid," J. Non-Newtonian Fluid Mech. **84**, 83–103 (1999).
[28] E. A. Brujan, "Cavitation bubble dynamics in non-Newtonian fluids," Polym. Eng. Sci. **49**, 419–431 (2009).
[29] J. Naude and F. Mendez, "Periodic and chaotic oscillations of a bubble gas immersed in an upper convective maxwell fluid," J. Non-Newtonian Fluid Mech. **155**, 30–38 (2008).
[30] Lord Rayleigh, "On the pressure developed in a liquid during the collapse of a spherical cavity," Philos. Mag. **34**, 94–98 (1917).
[31] J. B. Keller and M. Miksis, "Bubble oscillations of large amplitude," J. Acoust. Soc. Am. **68**, 628–633 (1980).
[32] A. Prosperetti and A. Lezzi, "Bubble dynamics in a compressible liquid. Part 1. First-order theory," J. Fluid Mech. **168**, 457–478 (1986).
[33] A. Lezzi and A. Prosperetti, "Bubble dynamics in a compressible liquid. Part 2. Second-order theory," J. Fluid Mech. **185**, 289–321 (1987).
[34] Y. C. Fung, *Biomechanics: Mechanical Properties of Living Tissues* (Springer-Verlag, Heidelberg, 1981).
[35] C. Zener, *Elasticity and Anelasticity of Metals* (University Press, Chicago, 1948).
[36] M. Orosz, G. Molnarka, and E. Monos, "Curve fitting methods and mechanical models for identification of viscoelastic parameters of vascular wall – Comparative study," Med. Sci. Monit. **3**, 599–604 (1997).
[37] S. Goss, R. L. Johnston, and F. Dunn, "Comprehensive compilation of empirical ultrasonic properties of mammalian tissues II," J. Acoust. Soc. Am. **68**, 93–108 (1980).
[38] A. Maxwell, C. A. Cain, T. L. Hall, J. B. Towlkes, and Z. Xu, "Probability of cavitation for single ultrasound pulses applied to tissues and tissue-mimicking materials," Ultrasound Med. Biol. **39**, 449–465 (2013).
[39] R. Apfel and C. Holland, "Gauging the likelihood of cavitation from short-pulse, low-duty cycle diagnostic ultrasound," Ultrasound Med. Biol. **17**, 179–185 (1991).
[40] E. L. Madsen, H. Sathoff, and H. J. Zagzebski, "Ultrasonic shear wave properties of soft tissues and tissuelike materials," J. Acoust. Soc. Am. **74**, 1346–1355 (1983).
[41] P. N. Wells and H. D. Liang, "Medical ultrasound: Imaging of soft tissue strain and elasticity," J. R. Soc., Interface **8**, 1521–1549 (2011).
[42] H. M. Loree, A. J. Grodzinsky, S. Y. Park, L. J. Gibson, and R. T. Lee, "Static circumferential tangential modulus of human atherosclerotic tissue," J. Biomech. **27**, 195–204 (1994).
[43] Z. Liu and L. Bilston, "On the viscoelastic character of liver tissue: Experiments and modelling of the linear behaviour," Biorheology **37**, 191–200 (2000).

[44] X. Yang and C. Church, "A simple viscoelastic model for soft tissues in the frequency range 6-20 MHz," IEEE Trans. Ultrason. Ferroelectr. Freq. Control **53**, 1404–1411 (2006).
[45] G. Holzapfel, *Nonlinear Solid Mechanics* (Wiley, New York, 2000).
[46] R. G. Larson, *Constitutive Equations for Polymer Melts and Solutions* (Butterworths, Boston, 1988).
[47] Z. Feng and L. G. Leal, "Nonlinear bubble dynamics," Annu. Rev. Fluid Mech. **29**, 201–243 (1997).
[48] W. Press, B. Flannery, S. A. Teukolsky, and W. T. Vetterling, *Numerical Recipes* (Cambridge University Press, 1992).
[49] A. H. Nayfeh and D. K. Mook, *Nonlinear Oscillations* (Wiley, New York, 1979).
[50] A. H. Nayfeh, *Perturbation Methods* (Wiley, New York, 1973).
[51] A. H. Nayfeh and W. S. Saric, "Nonlinear acoustic response of a spherical bubble," J. Sound Vib. **30**, 445–453 (1973).
[52] A. Francescutto and R. Nabergoj, "Steady-state oscillations of gas-bubbles in liquids - Explicit formulas for frequency-response curves," J. Acoust. Soc. Am. **73**, 457–460 (1983).
[53] A. Francescutto and R. Nabergoj, "A multiscale analysis of gas bubble oscillations: Transient and steady-state-solutions," Acustica **56**, 12–22 (1984).
[54] A. Prosperetti, "Nonlinear oscillations of gas-bubbles in liquids – Steady-state solutions," J. Acoust. Soc. Am. **56**, 878–885 (1974).
[55] A. Prosperetti, "Nonlinear oscillations of gas-bubbles in liquids – Transient solutions and connection between subharmonic signal and cavitation," J. Acoust. Soc. Am. **57**, 810–821 (1975).
[56] M. Minnaert, "On musical air-bubbles and the sound of running water," Philos. Mag. **16**, 235–248 (1933).